Mon. Not. R. Astron. Soc. **000**, 1–11 (2013) Printed 27 May 2014 (MN LATEX style file v2.2)

Galactic Globular and Open Cluster Fiducial Sequences in the Pan-STARRS1 Photometric System

Edouard J. Bernard,[1⋆] Annette M. N. Ferguson,[1] Edward F. Schlafly,[2] Imants Platais,[3] Eric F. Bell,[4] Nicolas F. Martin,[5,2] Hans-Walter Rix,[2] Colin T. Slater,[4] William S. Burgett,[6] Kenneth C. Chambers,[6] Peter W. Draper,[7] Klaus W. Hodapp,[6] Nicholas Kaiser,[6] Rolf-Peter Kudritzki,[6] Eugene A. Magnier,[6] Nigel Metcalfe,[7] John L. Tonry,[6] Richard J. Wainscoat,[6] Christopher Waters[6]

[1]*SUPA, Institute for Astronomy, University of Edinburgh, Royal Observatory, Blackford Hill, Edinburgh EH9 3HJ, UK*
[2]*Max-Planck-Institut für Astronomie, Königstuhl 17, D-69117 Heidelberg, Germany*
[3]*Department of Physics and Astronomy, Johns Hopkins University, 3400 North Charles Street, Baltimore, MD 21218, USA*
[4]*Department of Astronomy, University of Michigan, 500 Church St., Ann Arbor, MI 48109, USA*
[5]*Observatoire Astronomique de Strasbourg, Université de Strasbourg, CNRS, UMR 7550, 11 rue de l'Université, F-67000 Strasbourg, France*
[6]*Institute for Astronomy, University of Hawaii, 2680 Woodlawn Drive, Honolulu HI 96822, USA*
[7]*Department of Physics, Durham University, South Road, Durham DH1 3LE, UK*

arXiv:1405.6644v1 [astro-ph.GA] 26 May 2014

Accepted –. Received –; in original form –

ABSTRACT

We present the fiducial sequences of a sample of Galactic star clusters in the five bands of the Pan-STARRS1 (PS1) photometric system ($g_{\rm P1}$, $r_{\rm P1}$, $i_{\rm P1}$, $z_{\rm P1}$, and $y_{\rm P1}$). These empirical sequences – which include the red giant and sub-giant branches, the main sequence, and the horizontal branch – were defined from deep colour-magnitude diagrams reaching below the oldest main-sequence turn-offs of 13 globular and 3 old open clusters covering a wide range of metallicities ($-2.4 \lesssim [{\rm Fe/H}] \lesssim +0.4$). We find excellent agreement for the nine clusters in common with previous studies in similar photometric systems when transformed to the PS1 system. Because the photometric and spectroscopic properties of these stellar populations are accurately known, the fiducials provide a solid basis for the interpretation of observations in the PS1 system, as well as valuable constraints to improve the empirical colour–$T_{\rm eff}$ relations.

Key words: globular clusters: general – Hertzsprung-Russell diagram – globular clusters: individual (NGC 288, NGC 1904, NGC 4590, NGC 5272, NGC 5897, NGC 5904, NGC 6205, NGC 6341, NGC 6838, NGC 7078, NGC 7089, NGC 7099, Pal 12) – open clusters and associations: individual (NGC 188, NGC 2682, NGC 6791) – stars: evolution – surveys: Pan-STARRS1

1 INTRODUCTION

Since its introduction by the *Sloan Digital Sky Survey* (SDSS York et al. 2000), the *ugriz* photometric system has been widely adopted for optical observations, and adapted to the various instruments and needs of the surveys. In particular, the recent progress in deep-depletion CCD technology enhancing the quantum efficiency at the reddest wavelengths allows the addition of a y filter, which benefits greatly from being more immune to interstellar reddening – and therefore the possibility to peer deeper into the Milky Way disc – as well as higher temperature sensitivity for brown dwarfs studies and better constrained photometric redshifts. Thanks to the high throughput of the SDSS filters, it has become the reference system for many current and upcoming large sky surveys (e.g. Pan-STARRS1 (PS1): Kaiser et al. 2002, Large Synoptic Survey Telescope: Tyson 2002, Dark Energy Survey: The Dark Energy Survey Collaboration 2005, Subaru Hyper Suprime-Cam Project: Takada 2010, VST ALTAS: Shanks et al. 2013).

However, proper interpretation of the observed stellar populations depends on understanding the relation between the measured properties (e.g. colour, magnitude) and the physical properties (e.g. temperature, metallicity). One possibility is to compare directly the observations to stellar systems for which the properties are accurately known, such as globular and open clusters (GCs and OCs, respectively). It is also possible to use the observations of these

⋆ E-mail: ejb@roe.ac.uk

© 2013 RAS

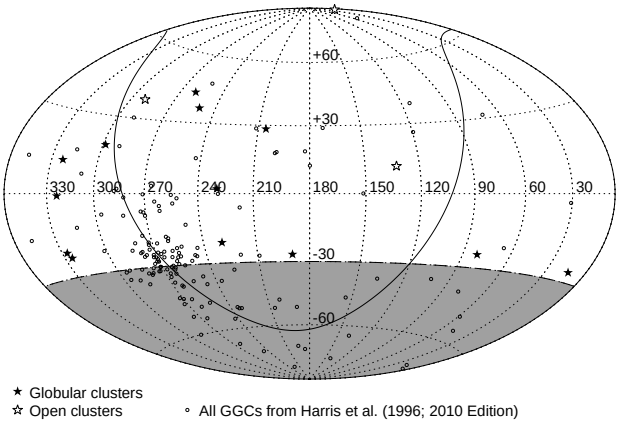

Figure 1. Distribution in equatorial coordinates of the globular clusters analysed in this work (filled stars), selected from the H10 catalogue of Galactic GCs (open circles). The three open clusters in our sample are shown as open stars. The solid line traces the Galactic disc, while the grayed area represents the fraction of the sky not observable from the PS1 3π telescope.

clusters as robust empirical constraints to improve theoretical models. For example, previous studies have highlighted the difficulty of fitting the colour-magnitude diagrams (CMDs) of Galactic GCs using the current stellar evolution libraries (e.g. VandenBerg & Clem 2003; Dotter et al. 2007; An et al. 2008; Brasseur et al. 2010), and the need for semi-empirical colour-temperature relations obtained from accurate star cluster fiducials (e.g. VandenBerg & Clem 2003, see also Salaris, Cassisi, & Weiss 2002).

We have taken advantage of the recently completed PS1 3π Survey (see below) to define a library of empirical fiducial sequences in the five bands of the PS1 photometric system ($g_{\rm P1}$, $r_{\rm P1}$, $i_{\rm P1}$, $z_{\rm P1}$, and $y_{\rm P1}$) based on deep observations of a sample of Galactic star clusters. Our goal is to use these fiducials for comparison with the stellar populations of the Milky Way halo, satellites, and globular clusters, hence the focus on old clusters. We briefly introduce PS1 in Section 2, and describe the photometry in Section 3. The cluster fiducials are defined and compared to literature values in Section 4. A summary is given in Section 5.

2 THE Pan-STARRS1 3π SURVEY

Pan-STARRS1 (Kaiser et al. 2010, K. C. Chambers et al., in preparation) is a 1.8 m optical telescope installed on the peak of Haleakala (Hawaii) and designed for dedicated survey observations. It is equipped with a 1.4-Gigapixel imager (Onaka et al. 2008; Tonry & Onaka 2009) covering a 7 square degree field-of-view ($\sim 3.3^\circ$ diameter). The 3π Survey, which forms the basis of the work presented here, covers 3/4 of the sky in five optical to near-infrared bands ($g_{\rm P1}r_{\rm P1}i_{\rm P1}z_{\rm P1}y_{\rm P1}$; Tonry et al. 2012).

With an exposure time ranging from 30 to 45 seconds, individual exposures have median 5σ limiting AB magnitudes of 21.9, 21.8, 21.5, 20.7, and 19.7 for the $g_{\rm P1}r_{\rm P1}i_{\rm P1}z_{\rm P1}y_{\rm P1}$bands, respectively (Morganson et al. 2012); saturation occurs at $\sim$13.5 for $g_{\rm P1}$, $r_{\rm P1}$, $i_{\rm P1}$, $\sim$13.0 for $z_{\rm P1}$, and $\sim$12.0 for $y_{\rm P1}$(Magnier et al. 2013). The whole sky visible from Hawaii is being observed four times per band and per year, over a period of about four years, which will lead to an increased depth of $\sim$1.2 mag on the final stacked images (Metcalfe et al. 2013). The median seeing is a function of wavelength, ranging from $1.0''$ in $y_{\rm P1}$ to $1.3''$ in $g_{\rm P1}$(Metcalfe et al. 2013). The individual frames are automatically processed with the Image Processing Pipeline (Magnier 2006) to produce a photometrically and astrometrically calibrated catalogue. In particular, the images are resampled to a uniform pixel size ($0.25''$) and aligned to the equatorial axes on regular areas on the sky (called *skycells*). These skycells are roughly 6250 pixels across ($\sim 26'$), and the resulting images are called *warps*.

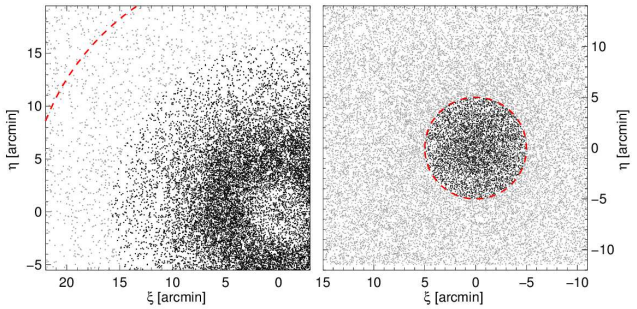

Figure 2. Spatial distribution, in standard coordinates, of the stars within the analysed skycell for globular cluster NGC 5904 (left) and open cluster NGC 6791 (right). Black and gray points represent the stars used to determine the cluster fiducial and the rejected stars, respectively. The dashed circle in each panel shows the characteristic radius r (see Table 1).

3 CLUSTER PHOTOMETRY

Using the 2010 Edition of the Harris (1996) catalogue of Galactic GCs (Harris 2010, hereafter H10), we count 96 known GCs located in the footprint of PS1 (i.e. $\delta > -30$; see Figure 1). Because the objective of our work is to obtain well-defined cluster fiducials over a wide range of magnitudes, including the main-sequence turn-off (MSTO), we limited our analysis to nearby, well-populated, and low foreground reddening clusters. All the clusters from H10 satisfying the following constraints were selected: $(m - M) < 16$, $\mathrm{E}(B - V) \leqslant 0.1$, and $\mathrm{M}_V < -6$. This reduced the list to eleven clusters. To extend the range of metallicities covered by the sample, we added NGC 6838 (M 71) and Pal 12, as well as the old open clusters NGC 188, NGC 6791, NGC 2682 (M 67). The properties of the whole sample are summarised in Table 1.

Because the Survey data reduction is still ongoing, neither the reduced images nor the photometric catalogues are final. At the beginning of this project the quality of the pipeline photometry in crowded regions was not optimal. It was thus decided to perform the stellar photometry on the PS1 images with the standard DAOPHOT/ALLSTAR/ALLFRAME suite of programs (Stetson 1994), which was specifically developed for crowded field photometry.

For each cluster (except NGC 188, see below) a single skycell was analysed; a region of $\sim$26' on a side is sufficient to sample a significant fraction of the area within the tidal radius of any cluster, regardless of their precise location within the skycell. Figure 2 shows the spatial distribution of stellar objects within the studied skycell for an extended (NGC 5904) and a more compact (NGC 6791) cluster. All the warps in all five bands of a given skycell were retrieved from the PS1 Science Interface[1]. Between 2 and 25 images per band were available for each cluster, with a median of 12 images per band.

[1] http://web01.psps.ifa.hawaii.edu

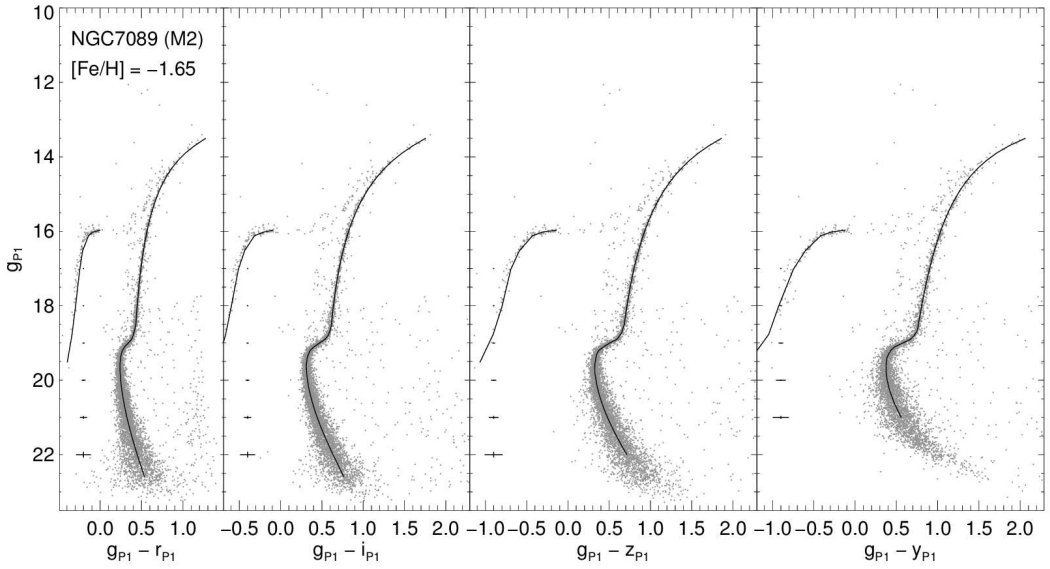

Figure 3. CMDs and corresponding fiducials for globular cluster NGC 7089.

Table 1. Properties of the globular and open clusters in our sample, from H10 (GCs) and Dias et al. (2002, OCs).

Name	Alt. Name	RA (J2000)	DEC (J2000)	[Fe/H]	E(B−V)	(m−M)	r^a (arcmin)
NGC 288	...	00 52 45.24	−26 34 57.4	−1.32	0.03	14.84	13.2
NGC 1904	M 79	05 24 11.09	−24 31 29.0	−1.60	0.01	15.59	8.0
NGC 4590	M 68	12 39 27.98	−26 44 38.6	−2.23	0.05	15.21	14.9
NGC 5272	M 3	13 42 11.62	+28 22 38.2	−1.50	0.01	15.07	28.7
NGC 5897	...	15 17 24.50	−21 00 37.0	−1.90	0.09	15.76	10.1
NGC 5904	M 5	15 18 33.22	+02 04 51.7	−1.29	0.03	14.46	23.6
NGC 6205	M 13	16 41 41.24	+36 27 35.5	−1.53	0.02	14.33	21.0
NGC 6341	M 92	17 17 07.39	+43 08 09.4	−2.31	0.02	14.65	12.4
NGC 6838	M 71	19 53 46.49	+18 46 45.1	−0.78	0.25	13.80	8.9
NGC 7078	M 15	21 29 58.33	+12 10 01.2	−2.37	0.10	15.39	27.3
NGC 7089	M 2	21 33 27.02	−00 49 23.7	−1.65	0.06	15.50	12.4
NGC 7099	M 30	21 40 22.12	−23 10 47.5	−2.27	0.03	14.64	19.0
Pal 12	...	21 46 38.84	−21 15 09.4	−0.85	0.02	16.46	19.1
NGC 188	...	00 47 28	+85 15 18	−0.03	0.08	11.56	8.5
NGC 2682	M 67	08 51 18	+11 48 00	+0.03	0.04	9.49	12.5
NGC 6791	...	19 20 53	+37 46 18	+0.42	0.16	13.51	5.0

^{a} the characteristic radius r represents the tidal radius for the GCs, and the apparent radius for the OCs.

We performed a first source detection at the 10-σ level on the individual warps, which was used as input for aperture photometry. From this catalogue, 200 bright, non-saturated stars per warp were selected as potential PSF stars; an automatic rejection based on the shape parameters was used to clean the lists. Modelling of the empirical PSF was done iteratively with DAOPHOT: the clean lists were used to remove all the stars from the warps except PSF stars, so that accurate PSFs could be created from non-crowded stars. At each iteration, the PSF was modeled more accurately and the neighbouring stars thus removed better. Every few iterations, the degree of PSF variability across the image was also increased, from constant to linear, then quadratically variable.

We then created a median, master image by stacking all the warps from all the bands using the stand-alone program MONTAGE2. This master image, free of chip gaps and much deeper than any individual frame, was used to create the input star list for ALLFRAME by performing a second source detection. The output of ALLFRAME consists of a catalogue of PSF photometry for each image. A robust mean magnitude was obtained for each star by combining these catalogues with DAOMASTER. The final photometry was calibrated to the PS1 system by matching our resulting catalogue to that produced and calibrated by the pipeline (see Schlafly et al. 2012) for the given skycell. Using several hundreds of stars in common in the uncrowded areas of the skycells, the residuals have a standard deviation $\lesssim$0.02 mag and show no trend with either magnitude or colour. The contribution of these transformations to the uncertainty of the individual magnitudes is therefore negligible ($\sim$0.001).

The photometry of NGC 188 was performed in a slightly different manner from the other clusters. It is located in a part of the sky for which the data was not fully processed by the pipeline yet, leading to two minor differences: (i) the warps were not available, so the photometry was carried out on the un-resampled, un-rotated

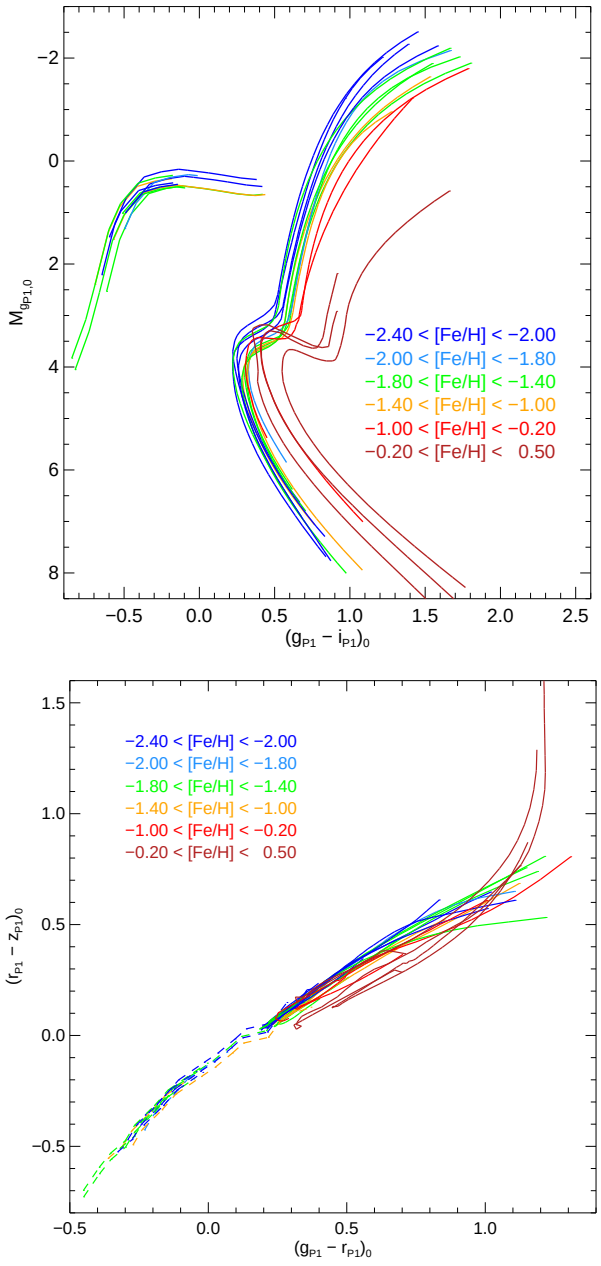

Figure 4. Comparison of the fiducials obtained for all the clusters, colour-coded by their metallicity as described in the insets, in a CMD (top) and colour-colour diagram (bottom). In the latter, the HBs are shown as dashed lines for clarity.

images of the cluster; and (ii) the photometric calibration is preliminary and may not be as accurate as for the other clusters.

The final step consisted of cleaning the photometric catalogues of non-stellar objects and blended stars in order to obtain a well-defined stellar locus. This was possible thanks to the photometric quality parameters returned by ALLFRAME (χ and *sharp*), as well as the separation index *sep* (see Stetson, Bruntt, & Grundahl 2003) to reduce the effects of photometric degradation due to crowding. Specifically, we used $|sharp| \leqslant 1.5$, *sep* $\geqslant 3.5$, and a magnitude dependent χ. To limit the number of foreground contaminants, we only included objects within ∼1/2–1 characteristic radius r (see Table 1), depending on the density of surrounding field stars. The CMDs of the open clusters NGC 188 and NGC 6791 were further cleaned by removing the foreground Milky Way stars based on their proper motions (Platais et al. 2003, 2011).

4 CLUSTER FIDUCIALS

4.1 Defining the Cluster Fiducials

To determine the cluster fiducials, we found that the $(g_{\rm P1} - X, g_{\rm P1})$ plane, where X represents one of the $r_{\rm P1}$, $i_{\rm P1}$, $z_{\rm P1}$, or $y_{\rm P1}$ filters, produced the best results since the MSTO is better defined by including bluer bands. Sample CMDs corresponding to these band combinations are shown in Figure 3.

For the red giant branch (RGB), sub-giant branch (SGB), and main sequence (MS), the fiducials were defined in a manner similar to that described in Marín-Franch et al. (2009). First, the sigma-clipped median colour is calculated for magnitude bins that have a size which varies as a function of the number of stars and the photometric errors, from 0.2 to 0.8 mag. These values define the preliminary ridge line. This is then refined between the MSTO and the base of the RGB by computing, at each ridge point, the distribution of stars in a stripe perpendicular to the ridge line. To obtain smoother fiducials, we separately fit the RGB and the MS below the turn-off with a function of the form:

$$y = a + bx + c/(x - d)$$

where x and y represent the magnitude and the colour, respectively (see Saviane et al. 2000)[2]. Finally, for the few clusters where the cluster locus is double valued in color for a given magnitude (e.g. the SGB of the open clusters), the fiducial was refined by hand.

Given the typically small number of stars on the horizontal-branch (HB) of individual clusters, we first created a robust HB fiducial by combining the HB stars of all the clusters together after correcting for the difference in distance and reddening. For each cluster, this fiducial was then simply offset in colour and magnitude, then trimmed to match the observed HB. Figure 3 shows the fiducials obtained in the various band combinations for NGC 7089, overplotted on the cleaned CMDs. The fiducials for the other clusters are shown in the Appendix, and are provided in tabular form available as Supporting Information with the online version of the paper.

In Figure 4 we present the fiducials of all the clusters colour-coded by their metallicity: the top and bottom panels show a CMD and a colour-colour diagram, respectively. The fiducials were converted to absolute magnitude and intrinsic colour assuming the distances and reddening from H10 and Dias et al. (2002), and the extinction in each band from Schlafly & Finkbeiner (2011). Note that the bright end of several fiducials do not include the tip of the RGB as stars brighter than $g_{\rm P1} \sim 13.5$ are saturated in the PS1 images. The CMDs clearly show the expected trend of redder colour and fainter sub-giant branch with increasing metallicity. A mild metallicity trend is also visible in the bottom panel; since this diagram is distance-independent, it may prove useful for constraining the metallicity of field stars.

[2] Note that Saviane et al. (2000) used the reverse notation, with x and y representing the colour and the magnitude, respectively

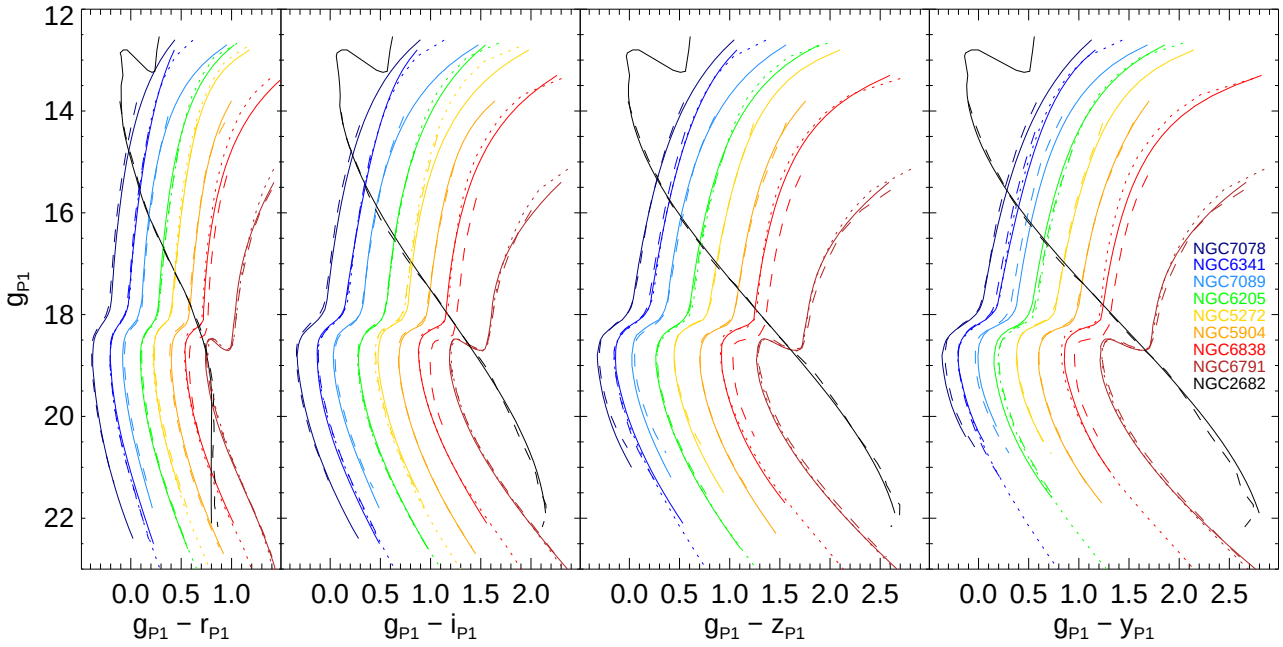

Figure 5. Comparison between the fiducials obtained in this work (solid lines) and those of the literature after transformation to the PS1 system: Clem et al. (dotted lines) and An et al. (dashed lines). The fiducials of individual clusters have been arbitrarily offset in colour and magnitude for clarity.

4.2 Comparison with Literature Fiducials

Given that the filter set has been designed specifically for PS1, there are no fiducials in the literature that are directly comparable to ours. However, fiducials have been obtained for a number of clusters in the SDSS $ugriz$ and CFHT/MegaCam $u'g'r'i'z'$ systems. The similarity of the PS1 filters to these allows the determination of robust transformations between the systems (see Tonry et al. 2012).

The first extensive set of fiducials was obtained by Clem, VandenBerg, & Stetson (2008). They secured very deep observations of four globular clusters and one open cluster with the CFHT. The combination of long and short exposure times allowed them to obtain high quality fiducials ranging from the tip of the RGB to roughly 4 magnitudes below the MSTO. All the clusters they analysed are included in our sample. The work of An et al. (2008) was carried out with the SDSS images. Since the standard SDSS photometric pipeline could not handle the high stellar density in and around Milky Way clusters, An et al. (2008) re-analysed the images around the 17 globular clusters found in the SDSS footprint, as well as three open clusters, with DAOPHOT/ALLFRAME. Seven globular and two open clusters are in common with ours.

We first converted the Clem, VandenBerg, & Stetson (2008) fiducials to the SDSS photometric system using the transformations from Tucker et al. (2006); both sets of fiducials were then transformed to the PS1 system using Equation 6 in Tonry et al. (2012). Note that the SDSS and CFHT filter sets do not have a y filter, so this is extrapolated from the z-band (see Tonry et al. 2012). Finally, we corrected the SDSS and CFHT r-band magnitudes for a systematic offset, in the sense that they appear too faint by 0.03 mag (Tonry et al. 2012, see also Fukugita et al. 2011).

The comparison is shown in Figure 5. The fiducials defined in this work are shown as solid lines, while the ones from Clem, VandenBerg, & Stetson (2008) and An et al. (2008) are shown as dashed and dotted lines, respectively. For magnitudes fainter than $g_{P1} \sim 14$, we find excellent agreement between the various sets (i.e. better than 0.02 mag in g_{P1}, r_{P1}, i_{P1}, and z_{P1}, and better than 0.06 mag in the y_{P1}-band) indicating that the photometric calibration and transformations between systems are accurate. The only exception is for NGC 6838 (M 71). An et al. (2008) already noted a $\sim$0.1 mag offset to the red compared to the fiducials of Clem, VandenBerg, & Stetson (2008), citing the difficulty to obtain a reliable calibration in a field with high stellar crowding which prevented the SDSS pipeline to measure a sufficient number of stars. Our fiducials for this cluster agree with the ones of Clem, VandenBerg, & Stetson (2008) and therefore confirm the problematic calibration of the NGC 6838 photometry of An et al. (2008).

5 CONCLUSIONS

We have obtained deep, homogeneous photometry of a sample of globular and open clusters covering a wide range of metallicities from images of the PS1 3π Survey. We used this photometry to derive fiducial sequences in the five bands of the PS1 photometric system. The comparison with literature fiducials in similar photometric systems shows very good agreement and therefore that the photometric calibration and transformations between systems are accurate.

These empirical isochrones, for which the photometric and spectroscopic properties are accurately known, can be used to characterize the properties of resolved stellar systems found in the footprint of PS1 and other surveys observing with the same filters, as well as to improve the empirical colour–$T_{\rm eff}$ relations predicted from model atmospheres.

ACKNOWLEDGMENTS

We are grateful to the anonymous referee for a constructive report. This research was supported by a consolidated grant from the

Science Technology and Facilities Council. E.F.S. and N.F.M. acknowledge support from the DFG's grant SFB881 (A3) "The Milky Way System". N.F.M. gratefully acknowledges the CNRS for support through PICS project PICS06183.

The PS1 Surveys have been made possible through contributions of the Institute for Astronomy, the University of Hawaii, the Pan-STARRS Project Office, the Max-Planck Society and its participating institutes, the Max Planck Institute for Astronomy, Heidelberg and the Max Planck Institute for Extraterrestrial Physics, Garching, The Johns Hopkins University, Durham University, the University of Edinburgh, Queen's University Belfast, the Harvard-Smithsonian Center for Astrophysics, the Las Cumbres Observatory Global Telescope Network Incorporated, the National Central University of Taiwan, the Space Telescope Science Institute, the National Aeronautics and Space Administration under Grant No. NNX08AR22G issued through the Planetary Science Division of the NASA Science Mission Directorate, the National Science Foundation under Grant No. AST-1238877, and the University of Maryland.

REFERENCES

An D., et al., 2008, ApJS, 179, 326
Brasseur C. M., Stetson P. B., VandenBerg D. A., Casagrande L., Bono G., Dall'Ora M., 2010, AJ, 140, 1672
Clem J. L., VandenBerg D. A., Stetson P. B., 2008, AJ, 135, 682
Dias W. S., Alessi B. S., Moitinho A., Lépine J. R. D., 2002, A&A, 389, 871
Dotter A., Chaboyer B., Jevremović D., Baron E., Ferguson J. W., Sarajedini A., Anderson J., 2007, AJ, 134, 376
Fukugita M., Yasuda N., Doi M., Gunn J. E., York D. G., 2011, AJ, 141, 47
Harris W. E., 1996, AJ, 112, 1487
Harris W. E., 2010, astro-ph/1012.3224 (H10)
Kaiser N., et al., 2002, Proc. SPIE, 4836, 154
Kaiser N., et al., 2010, Proc. SPIE, 7733, 77330E
Magnier E., 2006, in Ryan S., ed., The Advanced Maui Optical and Space Surveillance Technologies Conference, The Maui Economic Development Board, Hawaii, p. E50
Magnier E. A., et al., 2013, ApJS, 205, 20
Marín-Franch A., et al., 2009, ApJ, 694, 1498
Metcalfe N., et al., 2013, MNRAS, 435, 1825
Morganson E., et al., 2012, AJ, 143, 142
Onaka P., Tonry J. L., Isani S., Lee A., Uyeshiro R., Rae C., Robertson L., Ching G., 2008, Proc. SPIE, 7014, 12
Platais I., Cudworth K. M., Kozhurina-Platais V., McLaughlin D. E., Meibom S., Veillet C., 2011, ApJ, 733, L1
Platais I., Kozhurina-Platais V., Mathieu R. D., Girard T. M., van Altena W. F., 2003, AJ, 126, 2922
Salaris M., Cassisi S., Weiss A., 2002, PASP, 114, 375
Saviane I., Rosenberg A., Piotto G., Aparicio A., 2000, A&A, 355, 966
Schlafly E. F., et al., 2012, ApJ, 756, 158
Schlafly E. F., Finkbeiner D. P., 2011, ApJ, 737, 103
Shanks T., et al., 2013, Msngr, 154, 38
Stetson P. B., 1994, PASP, 106, 250
Stetson P. B., Bruntt H., Grundahl F., 2003, PASP, 115, 413
Takada M., 2010, in Kawai N. & Nagataki S., eds., Deciphering the Ancient Universe with Gamma-Ray Bursts, AIP Conf. Ser. 1279, Melville, NY: AIP, 120
The Dark Energy Survey Collaboration, 2005, astro-ph/0510346
Tonry J. L., et al., 2012, ApJ, 750, 99
Tonry J., Onaka P., 2009, in Ryan S., ed., The Advanced Maui Optical and Space Surveillance Technologies Conference, Red Hook, NYC: Curran & Associates, Inc., p. E40
Tucker D. L., et al., 2006, AN, 327, 821
Tyson J. A., 2002, in Tyson J. A. & Wolff S., eds., Survey and Other Telescope Technologies and Discoveries, Proc. SPIE, 4836, 10
VandenBerg D. A., Clem J. L., 2003, AJ, 126, 778
York D. G., et al., 2000, AJ, 120, 1579

APPENDIX A: FIDUCIALS

Figures A1–A15 present the CMDs and corresponding fiducials for the full sample of clusters analysed in this work. The fiducials are also provided in tabular form available as Supporting Information with the online version of the paper.

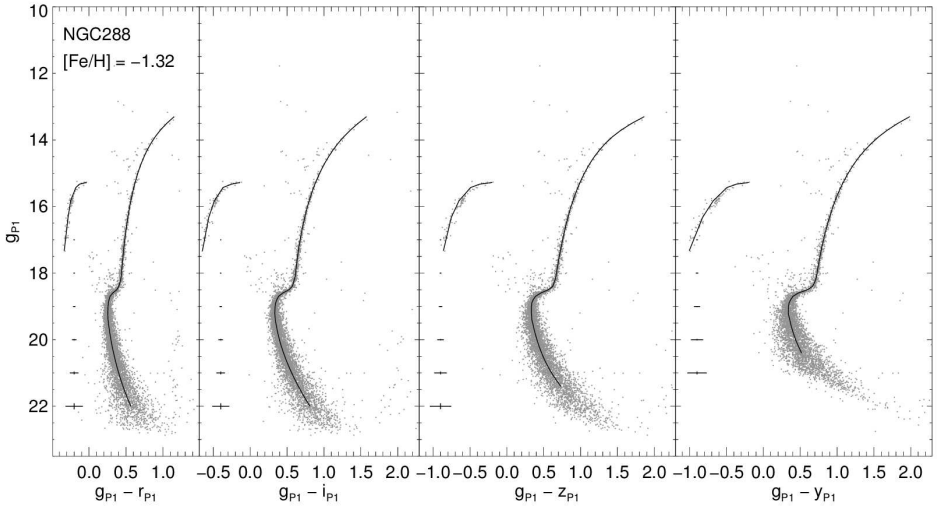

Figure A1. CMDs and corresponding fiducials for globular cluster NGC 288.

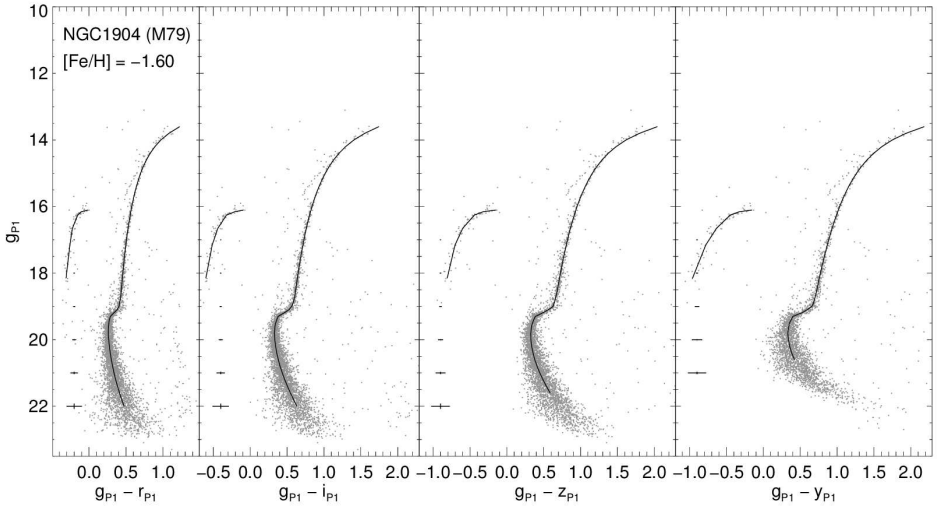

Figure A2. Same as in Figure A1, for NGC 1904 (M 79).

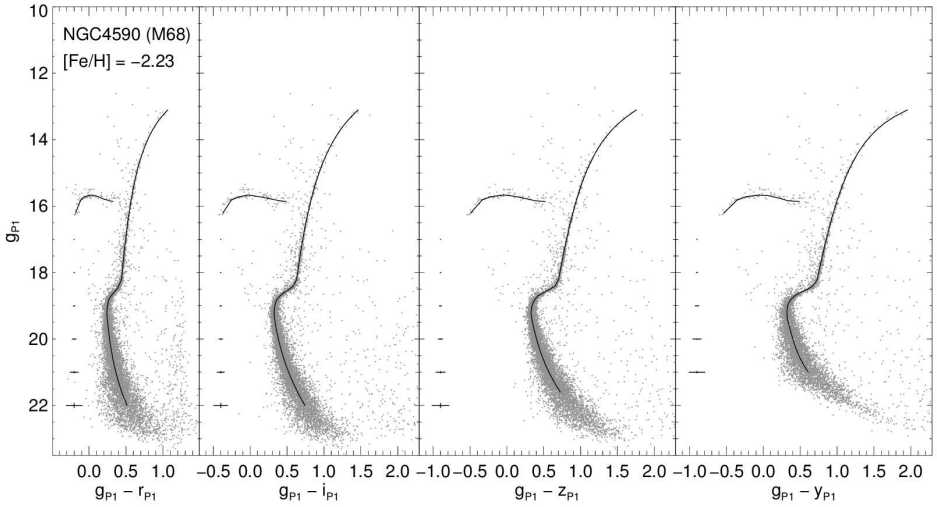

Figure A3. Same as in Figure A1, for NGC 4590 (M 68).

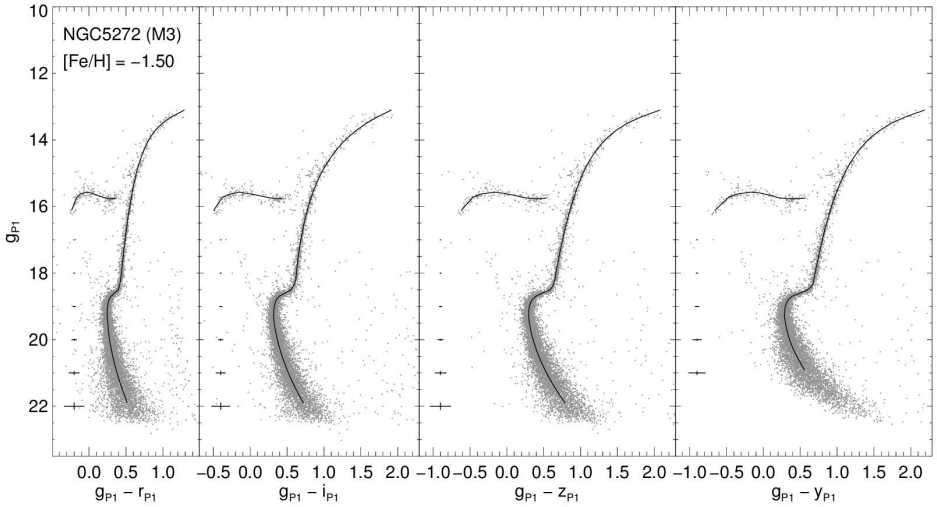

Figure A4. Same as in Figure A1, for NGC 5272 (M 3).

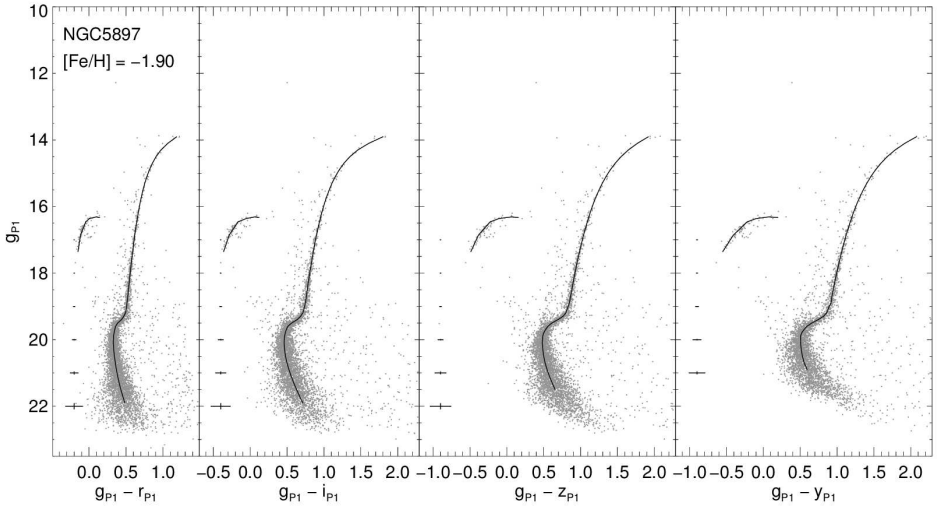

Figure A5. Same as in Figure A1, for NGC 5897.

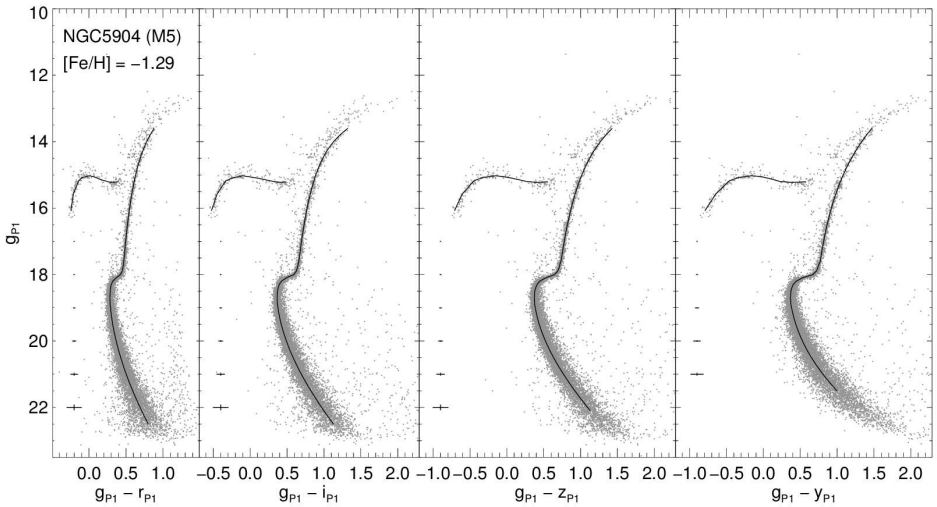

Figure A6. Same as in Figure A1, for NGC 5904 (M 5).

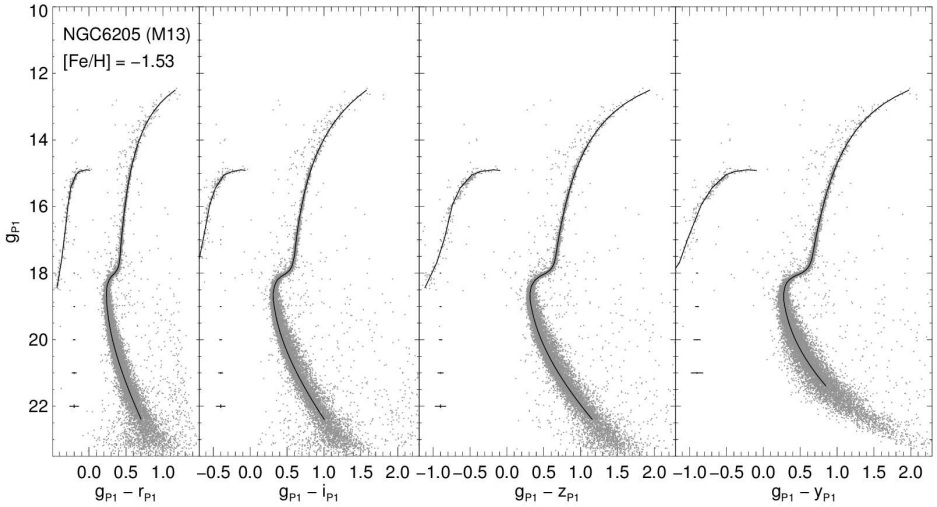

Figure A7. Same as in Figure A1, for NGC 6205 (M 13).

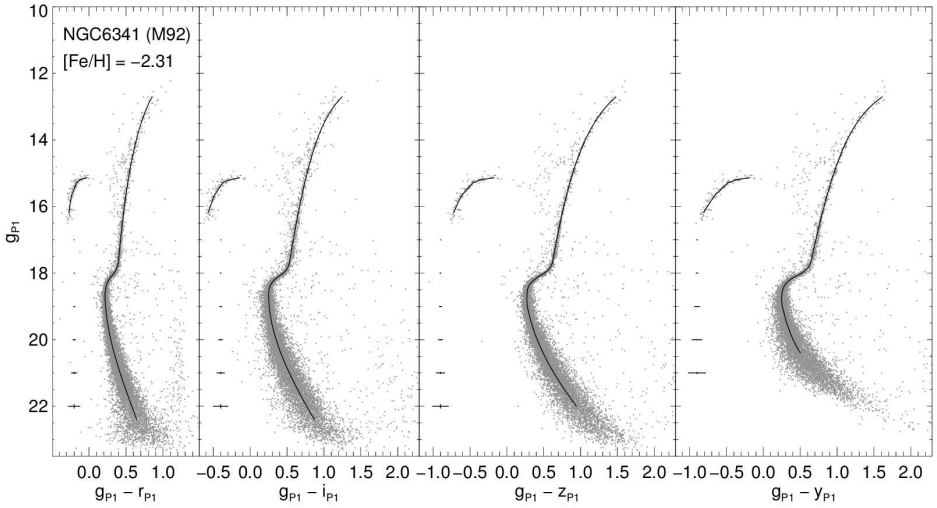

Figure A8. Same as in Figure A1, for NGC 6341 (M 92).

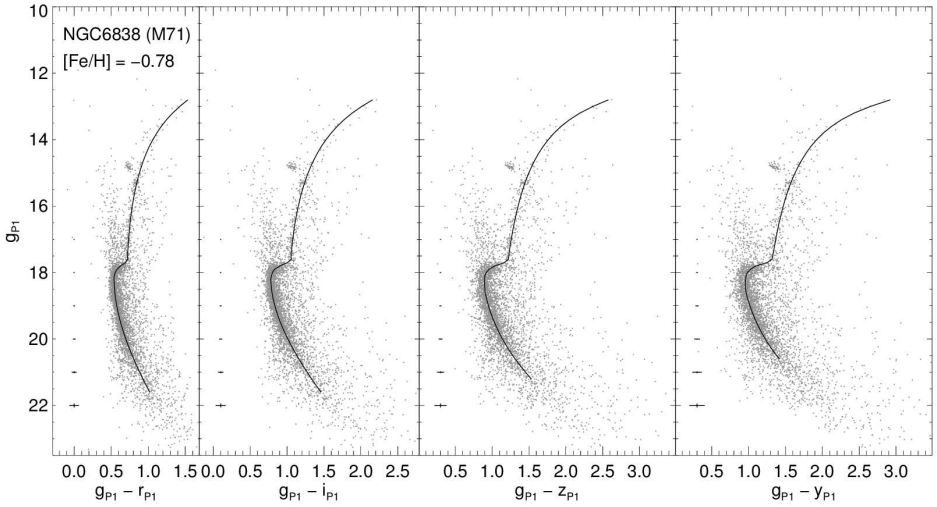

Figure A9. Same as in Figure A1, for NGC 6838 (M 71).

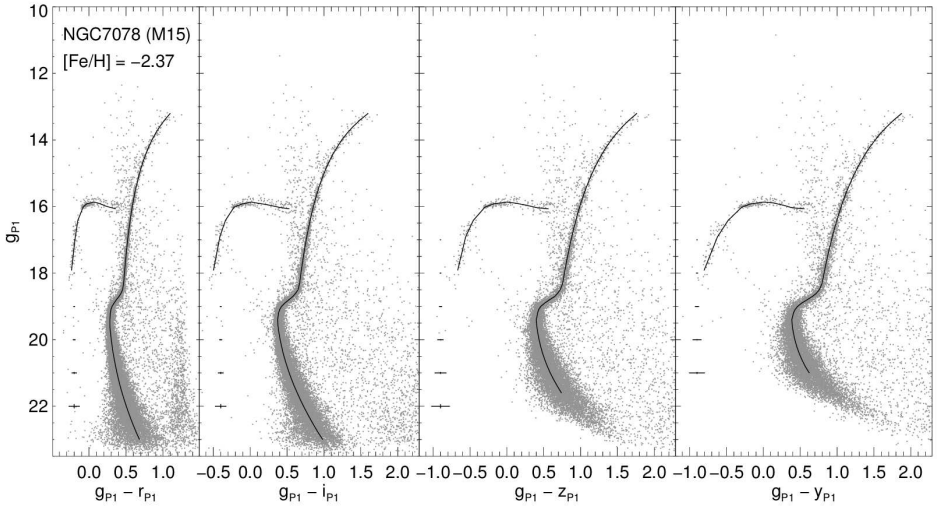

Figure A10. Same as in Figure A1, for NGC 7078 (M 15).

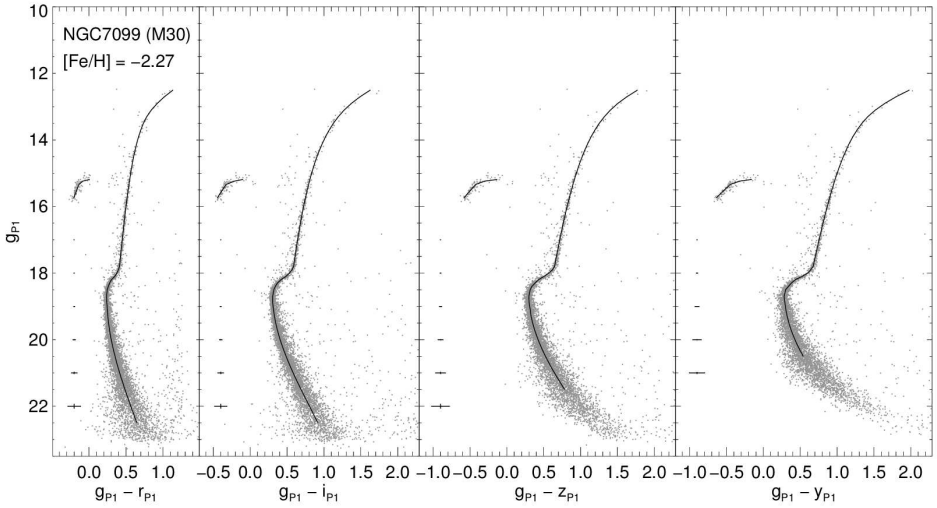

Figure A11. Same as in Figure A1, for NGC 7099 (M 30).

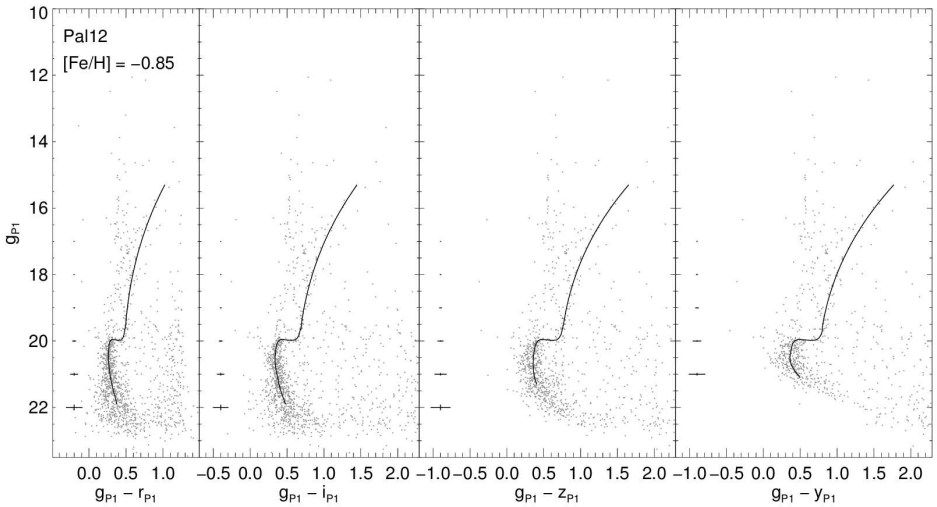

Figure A12. Same as in Figure A1, for Pal 12.

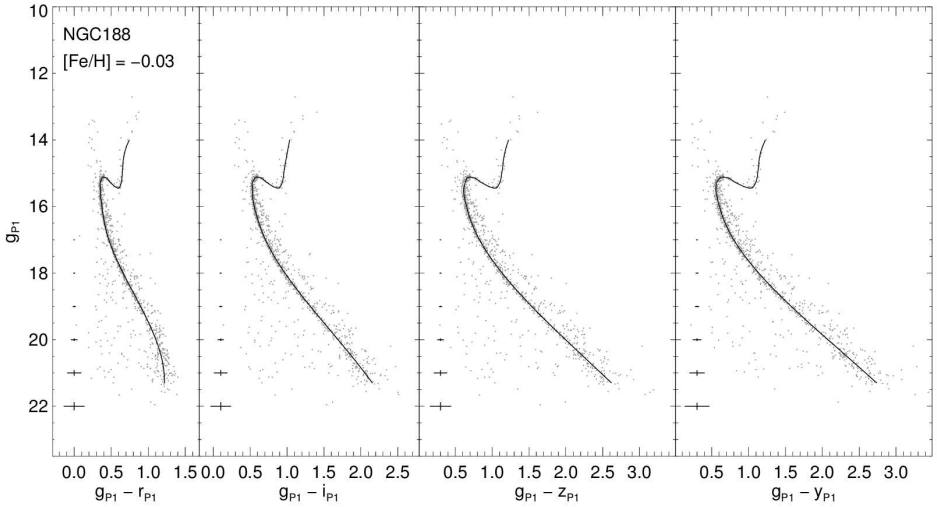

Figure A13. Same as in Figure A1, for open cluster NGC 188.

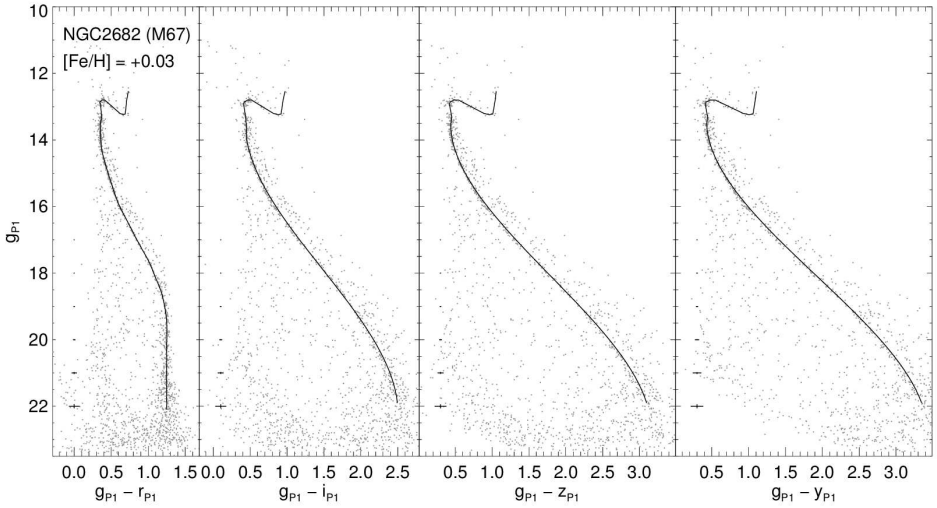

Figure A14. Same as in Figure A13, for NGC 2682 (M 67).

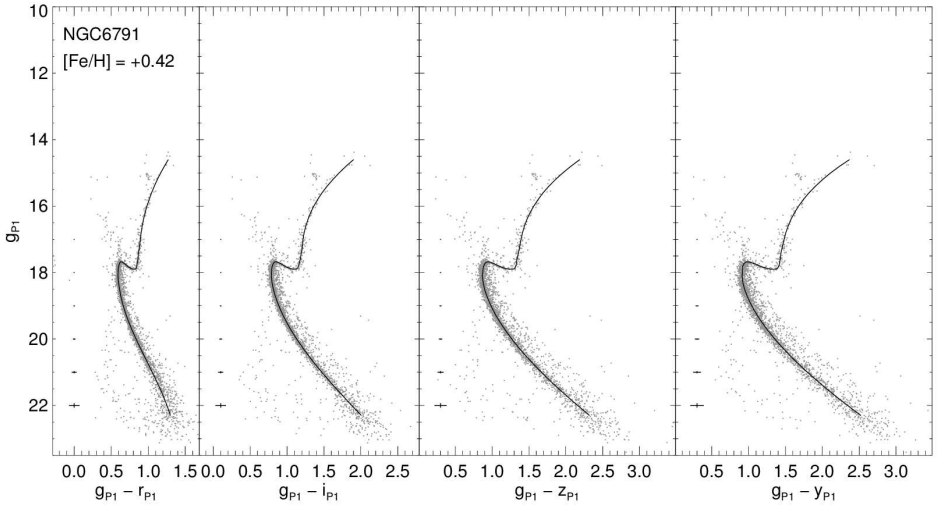

Figure A15. Same as in Figure A13, for NGC 6791.